HHS Public Access

Author manuscript

Sci Signal. Author manuscript; available in PMC 2016 August 22.

Published in final edited form as:

Sci Signal. ; 7(340): ra82. doi:10.1126/scisignal.2005287.

Diacylglycerol kinase-α controls T cell polarity by shaping diacylglycerol accumulation at the immune synapse

Anne Chauveau[1], **Audrey Le Floc'h**[1], **Niels S. Bantilan**[1], **Gary A. Koretzky**[2], and **Morgan Huse**[1,*]

[1]Immunology Program, Memorial Sloan-Kettering Cancer Center, New York, NY, USA

[2]Abramson Family Cancer Research Institute, Perelman School of Medicine, University of Pennsylvania, Philadelphia, PA, USA

Abstract

Polarization of the T cell microtubule-organizing center (MTOC) to the immunological synapse maintains the specificity of effector responses by enabling directional secretion toward the antigen-presenting cell. MTOC reorientation is guided by a sharp gradient of diacylglycerol that is centered at the synapse. Here, we used a single cell photoactivation approach to demonstrate that diacylglycerol kinase-α (DGK-α) controls T cell polarity by limiting the diffusion of diacylglycerol. DGK-α deficient T cells exhibited enlarged synaptic diacylglycerol accumulations and impaired MTOC reorientation. By contrast, T cells lacking the related isoform DGK-ζ did not display polarization defects. We also found that DGK-α localized preferentially to the periphery of the synapse, suggesting that it constrains the scope of diacylglycerol accumulation from the outside. Phosphoinositide 3-kinase activity was required for this peripheral localization pattern, establishing an intriguing link between diacylglycerol and phosphatidylinositol signaling during T cell activation. These results reveal a previously unappreciated function of DGK-α and provide insight into the mechanisms of lymphocyte polarity.

Introduction

Cell polarity plays a central role in migration, asymmetric division, and intercellular communication. As such, it is essential for both the development and the homeostasis of complex tissues. In many cell types, polarized cellular architecture is dictated by the movement of the centrosome (also called the microtubule-organizing center, or MTOC) to one side of the cell. This event realigns the microtubule cytoskeleton, positions key

*Correspondence: husem@mskcc.org.

Supplementary Materials

Fig. S1. Photoactivatable ligands for the 5C.C7 and OT-1 TCRs.
Fig. S2. DGK-α is required for MTOC polarization in TCR photoactivation experiments.
Fig. S3. Synaptic localization patterns of DGK-α mutants.
Fig. S4. PI3K activity regulates MTOC polarization and synaptic DAG.
Movie S1. Localized TCR photoactivation induces MTOC reorientation.
Movie S2. DGK-ζ is dispensable for MTOC reorientation.
Movie S3. DGK-α is required for MTOC reorientation.
Movie S4. Localized TCR photoactivation induces focal DAG accumulation.
Movie S5. DGK-α is required for proper DAG gradient formation.

organelles, and is required for the elaboration of axons, primary cilia, and other specialized signaling structures (1). In lymphocytes such as T cells, B cells, and natural killer (NK) cells, the MTOC reorients toward the immunological synapse (IS) that forms between the lymphocyte and its stimulatory target cell (2). This event brings the Golgi apparatus, secretory lysosomes, and other vesicular compartments associated with the MTOC into close apposition with the synaptic membrane, thereby enabling the directional secretion of soluble factors toward the target cell. In this manner, MTOC polarization maintains the specificity and the precision of cytokine-mediated communication and cytotoxic killing.

Reorientation of the MTOC is triggered by engagement of the T cell antigen receptor (TCR) with cognate peptide-major histocompatibility complex (pMHC) molecules on the surface of the antigen-presenting target cell (APC) (2). This induces a membrane proximal tyrosine kinase cascade leading to the activation of several key signaling enzymes, among them phospholipase-Cγ (PLCγ), which hydrolyzes phosphatidylinositol 4,5 bisphosphate to yield two second messengers, inositol trisphosphate and diacylglycerol (DAG). Whereas IP_3 diffuses into the cytoplasm to promote calcium (Ca^{2+}) signaling, DAG accumulates in the plasma membrane, where it activates both Ras and protein kinase C (PKC) dependent signaling by recruiting proteins that contain typical C1 domains. DAG also forms a striking intracellular gradient that is centered at the IS (3). We have shown that this gradient serves as the polarizing signal to drive MTOC reorientation (4), and that it does so at least in part by recruiting three distinct PKC isozymes to the IS in an ordered cascade (5). Perturbations that disrupt the shape or the stability of the DAG gradient compromise MTOC polarization (4), strongly suggesting that controlling the scope of DAG signaling is crucial for this response.

The mechanisms that shape DAG accumulation at the IS are largely unknown, but there are indications that they involve not only the regulated production of DAG but also its regulated destruction (4). In that regard, enzymes that metabolize DAG or convert it to another species represent intriguing candidates for the regulation of T cell polarity. In multiple cell types, DAG signaling is opposed by DAG kinases (DGKs), a family of enzymes that phosphorylate DAG to yield phosphatidic acid (PA) (6, 7). The predominant members of this family in T cells are DGK-α and DGK-ζ. Studies to date using DGK-$\alpha^{-/-}$ or DGK-$\zeta^{-/-}$ mice have suggested that the two enzymes play partially redundant roles in the attenuation of DAG signaling during T cell activation (8–11). However, DGK-α and DGK-ζ display marked differences in structure both N- and C-terminal to their respective catalytic domains, implying that they might also have isoform-specific functions.

Whether DGK-α and DGK-ζ influence T cell polarity by shaping synaptic DAG accumulation is not known. In the present study, we investigated this issue using a combination of single cell imaging and targeted loss-of-function. Our results reveal an important role for DGK-α, but not DGK-ζ, in synaptic DAG gradient formation and MTOC reorientation.

Results

DGK-α, but not DGK-ζ, is required for MTOC polarization

To assess the importance of DGKs for MTOC polarization to the IS, we used primary $CD4^+$ T cell blasts isolated from DGK-$\alpha^{-/-}$ or DGK-$\zeta^{-/-}$ mice expressing the 5C.C7 TCR, which recognizes the moth cytochrome $C_{88–103}$ (MCC) peptide bound to the class II MHC molecule I-E^k. These cells were allowed to form conjugates with CH12 B cells loaded with MCC, and then fixed and stained for CD4 and pericentrin, a marker of the MTOC (Fig. 1A). Conjugates containing wild type T cells derived from littermate control mice were prepared in parallel for comparison. MTOC polarization toward the APC was quantified by calculating a “polarization index” equal to the distance between the IS and the MTOC divided by the distance between the IS and the back of the T cell. This analysis revealed a substantial defect in DGK-$\alpha^{-/-}$ T cells, with average polarization indices increasing ~65% relative to wild type controls (Fig. 1, A and B). Most of this change could be attributed to T cells displaying a partially polarized phenotype in which the MTOC reoriented toward the APC, but did not become tightly apposed to the IS. By contrast, polarization responses in DGK-$\zeta^{-/-}$ T cells were indistinguishable from wild type controls (Fig. 1, A and C), indicating that the two DGK isoforms operate in a nonredundant manner in this context.

To investigate the effects of DGK deficiency on MTOC dynamics more closely, we employed a single cell TCR photoactivation approach that enables both the induction and the imaging of polarization responses with high spatiotemporal resolution (12). Briefly, T cells are attached to glass surfaces coated with immobilized I-E^k containing a photoactivatable version of the MCC peptide (NPE-MCC) that is nonstimulatory until exposed to UV light (fig. S1A). Then, UV irradiation of a micron-scale region of the surface beneath an individual T cell is used to induce localized TCR activation. This typically results in recruitment of the MTOC to the stimulatory region within two minutes (4), where it remains for the duration of the imaging experiment (usually 8 minutes total).

DGK-$\zeta^{-/-}$ T cells behaved normally in this assay, polarizing to a similar extent as T cells derived from wild type littermate control mice (Fig. 2, A and B; Movie S1 and S2). By contrast, T cells lacking DGK-α often failed to reorient properly despite apparent attempts to do so (Fig. 2, A and C; Movie S1 and S3). Indeed, the average distance between the irradiated region and the MTOC was significantly higher in DGK-$\alpha^{-/-}$ T cells than in wild type controls (Fig. 2C). This was particularly obvious during the second half of time-lapse experiments, when the MTOC had typically settled at its new position. Analysis of individual MTOC trajectories revealed that DGK-$\alpha^{-/-}$ T cells often reoriented to positions either short of or beyond the irradiated region (fig. S2). This marked imprecision was consistent with a role for DGK-α in focusing the polarization response.

Next, we investigated whether DGK-α plays a similar role in $CD8^+$ T cells, using as our model system CTLs expressing the OT-1 TCR. To perform polarization experiments with these cells, we developed a photocaged form of their cognate ligand, the $ovalbumin_{257–264}$ peptide (SIINFEKL, call OVA hereafter) bound to the class I MHC protein H2-K^b (fig. S1B). With this reagent in hand, we were able to induce robust polarization responses in wild type CTLs. These responses were markedly impaired, however, in DGK-$\alpha^{-/-}$ CTLs,

which failed to properly reorient toward the irradiated region (Fig. 2D). This phenotype was similar to what we observed in $CD4^+$ T cells, implying a conserved role for DGK-α in both cell types.

Importantly, the polarization defect observed in DGK-$\alpha^{-/-}$ T cells was reversed by expression of full length DGK-α, demonstrating that the loss-of-function phenotype was specific (Fig. 3A). Furthermore, expression of a kinase dead point mutant of DGK-α (KD DGK-α) failed to rescue MTOC reorientation (Fig. 3A), indicating that the catalytic activity of the enzyme is required for polarity induction. Overexpression of DGK-ζ was also ineffective at reversing the DGK-$\alpha^{-/-}$ phenotype (Fig. 3B), lending further support to the interpretation that the two isoforms operate nonredundantly in this context. Taken together, these data demonstrate that DGK-α, but not DGK-ζ, is required for MTOC polarization in both $CD4^+$ and $CD8^+$ T cells.

DGK-α shapes the synaptic DAG gradient

Given the importance of localized DAG signaling for MTOC reorientation and the capacity of DGKs to control DAG levels, we reasoned that DGK-α might influence polarization responses by controlling the scope of DAG accumulation at the IS. To test this hypothesis, we analyzed wild type, DGK-$\alpha^{-/-}$, and DGK-$\zeta^{-/-}$ 5C.C7 T cells expressing a fluorescent biosensor for DAG comprising the tandem C1 domains of PKCθ fused to GFP (C1θ-GFP). These cells were stimulated on supported lipid bilayers containing I-E^k-MCC together with B7.1 and ICAM-1, which are ligands for the costimulatory receptor CD28 and the integrin LFA-1, respectively. After 10 minutes, they were fixed, stained for filamentous actin (F-actin), and imaged by TIRF microscopy. Under these conditions, T cells form radially symmetric synapses with the bilayer that are bounded by a peripheral ring of F-actin (13). In wild type cells, C1θ-GFP localized within this F-actin ring (Fig. 4A), indicating that the DAG gradient was constrained to the center of the IS. We quantified this result by dividing the diameter of the C1θ-GFP distribution by the diameter of the IS. This yielded a ratio of less than one (Fig. 4B), consistent with a centralized DAG distribution. A similar pattern of C1θ-GFP recruitment was observed in the absence of DGK-ζ (Fig. 4, A and B), suggesting that this isoform does not influence the compartmentalization of synaptic DAG. In DGK-$\alpha^{-/-}$ T cells, however, the DAG distribution was significantly broader, with C1θ-GFP invading the peripheral space occupied by F-actin (Fig. 4, A and B). We observed a similar phenotype in DGK-$\alpha^{-/-}$ OT-1 CTLs stimulated on bilayers containing H2-K^b-OVA (see Fig. 7), indicative of an analogous role for DGK-α in $CD8^+$ T cells. These results indicate that DGK-α, but not DGK-ζ, is required for shaping DAG accumulation at the IS, and further support the interpretation that DGK-α plays a unique role during polarity induction.

We also analyzed the scope of DAG accumulation in TCR photoactivation experiments. C1θ-GFP recruitment is typically observed at the plasma membrane within ~90 seconds of stimulation, and remains roughly localized to the irradiated region over the course of the experiment (4) (Fig. 4C; Movie S4). The degree to which this response is compartmentalized can be measured by calculating the normalized autocorrelation width of the C1θ-GFP distribution (see Materials and Methods). This parameter typically decreases after photoactivation (Fig. 4D), indicating that the overall distribution of DAG becomes more

focused after localized stimulation of the TCR. Photoactivation of DGK-α$^{-/-}$ T cells induced robust recruitment of C1θ-GFP that was comparable in magnitude to the response observed in wild type cells (Fig. 4C; Movie S5). This recruitment response, however, was not well localized to the irradiated region, and there was no corresponding decrease in normalized autocorrelation width after photoactivation (Fig. 4D). Hence, DGK-α$^{-/-}$ T cells displayed a specific defect in their ability to constrain the DAG gradient. We observed similar results using both 5C.C7 and OT-1 T cells (Fig. 4D), although the effects of DGK-α deficiency were less pronounced in the OT-1 system. In general, OT-1 photoactivation experiments tended to be noisier than analogous 5C.C7 experiments, possibly due to low-level, UV-independent stimulation of the OT-1 TCR by photocaged H2-K^{b}-OVA. Nevertheless, when taken together with the lipid bilayer studies described above, these data strongly suggest that DGK-α limits the scope of synaptic DAG accumulation in both CD4^{+} and CD8^{+} T cells.

DGK-α deficiency enhances downstream signaling but not cytotoxicity

DGK-α deficiency has been reported to enhance DAG dependent signaling and cytokine secretion in both naïve and effector T cells (8, 9, 11, 14, 15). Consistent with this prior work, we found that DGK-α$^{-/-}$ 5C.C7 T cell blasts released substantially more IL-2 than wild type controls after stimulation with antibodies against CD3 and CD28 (Fig. 5A). Loss of DGK-α, however, had no significant effect on target cell killing by OT-1 CTLs (Fig. 5B). This was rather surprising given that DGK-α$^{-/-}$ CTLs exhibited amplified TCR-induced Erk1/2 phosphorylation at early time points (Fig. 5C and 5D). Previous studies have established the importance of MTOC reorientation for optimal cytotoxic responses (4, 16–19). Hence, the potential gains in cytotoxicity resulting from enhanced DAG signaling are likely to be offset by suboptimal polarization toward the IS.

DGK-α localizes to the periphery of the IS

It has been shown that TCR activation induces the recruitment of both DGK-α and DGK-ζ to the plasma membrane (20–23). The compartmentalization of each protein within the IS, however, has not been examined. To address this issue, we prepared OT-1 CTLs that expressed GFP-labeled forms of DGK-α or DGK-ζ. These cells were stimulated on bilayers containing ICAM-1, H-2K^{b}-OVA, and B7.1, stained for F-actin, and imaged by TIRF microscopy. DGK-α accumulated preferentially in the periphery of the IS, where it displayed substantial overlap with the F-actin ring (Fig. 6A). By contrast, DGK-ζ was distributed in a uniform manner over the entire synaptic membrane (Fig. 6A). We quantified the annularity of these localization patterns by calculating the ratio between the average fluorescence intensity in the center of the IS and the average fluorescence intensity in the periphery. This analysis revealed a statistically significant difference between DGK-α and DGK-ζ (Fig. 6B). Intriguingly, the annular configuration adopted by DGK-α was essentially reciprocal to the centralized pattern we observed for C1θ-GFP (Fig. 4A), suggesting that DGK-α might constrain the scope of DAG accumulation from the outside.

Recruitment of DGK-α to the plasma membrane is controlled by its N-terminal regulatory region, which contains a recoverin homology domain, two Ca^{2+}-binding EF hands, and two atypical C1 domains that do not recognize DAG (21, 22, 24). The EF-hands are thought to

endow DGK-α with Ca^{2+} responsiveness by inhibiting membrane localization and enzymatic activity in the absence of Ca^{2+} (21). The C1 domains, for their part, are known to be required for membrane binding (24). To assess the relative importance of these domains for compartmentalization within the IS, we analyzed two deletion mutants, one lacking the recoverin homology domain and EF hands (ΔEF DGK-α), and one lacking the entire N-terminal regulatory region (ΔEF2C1 DGK-α) (fig. S3A). The δEF DGK-α localization pattern was similar to that of full length DGK-α (Fig. 6B and fig. S3B), indicating that the EF and recoverin homology domains are dispensable for enrichment at the periphery of the IS. By contrast, ΔEF2C1 DGK-α exhibited weak membrane recruitment and no peripheral enrichment (Fig. 6B and fig. S3B). Together, these results indicate that DGK-α compartmentalization within the IS requires the tandem C1 domains. In certain experimental systems, membrane recruitment of DGK-α is regulated by its own enzymatic activity (21, 24). However, we found that the synaptic localization of KD DGK-α was indistinguishable from that of the wild type protein (Fig. 6B and fig. S3B), arguing against a role for DAG turnover in this context.

To explore the relationship between DGK localization and the regulation of MTOC reorientation, we performed TCR photoactivation experiments using DGK-$\alpha^{-/-}$ T cells that had been transduced with ΔEF DGK-α or ΔEF2C1 DGK-α. Expression of δEF DGK-α rescued MTOC polarization to a similar extent as full length DGK-α (Fig. 6C), suggesting that regulation by the EF hands is not required for DGK-α dependent polarity induction. By contrast, ΔEF2C1 DGK-α failed to reverse the DGK-$\alpha^{-/-}$ phenotype (Fig. 6D). Hence, constructs exhibiting peripheral localization at the IS were in general capable of potentiating MTOC polarization. The exception of course was KD DGK-α, which localized to the periphery but lacked catalytic activity (Fig. 3A and Fig. 6B). Taken together, these results suggest that annular accumulation of DGK-α in the synaptic membrane is required for its effects on T cell polarity.

PI3K regulates synaptic DGK-α localization and MTOC reorientation

The apparent importance of peripheral DGK-α accumulation prompted us to investigate the signaling pathways controlling this localization behavior. Previous attention has focused on the role of intracellular Ca^{2+} (21, 22). We have shown, however, that Ca^{2+} signaling is dispensable for TCR-induced MTOC reorientation (4), implying the existence of other mechanisms for controlling DGK-α localization at the IS. In that regard, it is known that PI3K signaling can drive membrane recruitment of DGK-α in the absence of Ca^{2+} flux and that PIP_3, the product of PI3K, can directly induce DGK-α activation (25). This observation is particularly intriguing in light of recent data showing that PIP_3 also accumulates in an annular pattern at the periphery of the IS (26).

To assess the importance of PI3K signaling for DGK-α localization in our system, we treated OT-1 CTLs expressing GFP-labeled DGK-α with wortmannin, a small molecule PI3K inhibitor. The cells were then applied to stimulatory bilayers and imaged by TIRF microscopy. Wortmannin completely disrupted the peripheral accumulation of DGK-α (Fig. 6, E and F), yielding a uniform fluorescence distribution across the synaptic membrane.

These results strongly suggest that PI3K signaling is required for compartmentalization of DGK-α at the IS.

One would expect that disrupting DGK-α localization in this manner would also alter the synaptic DAG gradient. To test this hypothesis, we inhibited PI3K in OT-1 CTLs expressing C1θ-GFP and then imaged the cells on stimulatory bilayers. Wortmannin induced substantial broadening in the synaptic distribution of C1θ-GFP (Fig. 7A and 7B). This phenotype was similar to that seen in DGK-$\alpha^{-/-}$ T cells, suggesting that peripheral localization of DGK-α is crucial for constraining DAG to the IS. Consistent with this interpretation, wortmannin treatment also impaired MTOC polarization in TCR photoactivation experiments (Fig. 7C and fig. S4A). As we had observed for DGK-$\alpha^{-/-}$ T cells, this defect was associated with imprecise targeting of the MTOC to the irradiated region after reorientation (fig. S4B). Taken together, our data strongly suggest that PI3K signaling regulates MTOC polarization by influencing the localization of DGK-α at the IS.

Studies suggest that class IA PI3K family members, primarily PI3Kδ, are responsible for synaptic PIP_3 production (27, 28). To assess the role of PI3Kδ in DAG dependent polarity signaling, we made use of IC87114, a specific inhibitor of this isoform. IC87114-treated cells exhibited DAG gradient broadening and impaired MTOC reorientation (fig. S4C and S4D), similar to the effects of wortmannin. We conclude that PI3Kδ dependent PIP_3 production regulates DAG accumulation and cytoskeletal polarization at the IS.

Discussion

Although it has been known for some time that DGK activity attenuates DAG dependent signaling in T cells, the function of specific DGK isoforms remains poorly understood. Here, we demonstrate that DGK-α influences MTOC polarization toward the APC by constraining the scope of synaptic DAG accumulation. DGKs have generally been viewed as negative regulators of lymphocyte responses. However, by promoting cytoskeletal polarity, DGK-α exerts an important and decidedly positive effect on T cell activation and subsequent effector function. In that regard, it is probably worth re-evaluating the role of this enzyme within the TCR signaling cascade.

Prior work has suggested substantial functional overlap between DGK-α and DGK-ζ. DGK-$\alpha^{-/-}$ and DGK-$\zeta^{-/-}$ T cells display phenotypic similarities that include enhanced MAP kinase signaling and resistance to anergy (9, 14, 29). Furthermore, mice lacking both isoforms exhibit a block in thymocyte maturation that is not observed in either single knockout, implying redundant roles in T cell development (8). There are indications, however, that DGK-α and DGK-ζ might regulate DAG in different ways. DGK-$\zeta^{-/-}$ T cells display more pronounced dysregulation of the MAP kinase pathway than their DGK-$\alpha^{-/-}$counterparts (8, 9, 14). Furthermore, overexpression of DGK-ζ in Jurkat cells attenuates TCR-induced DAG production to a greater extent than DGK-α (20). Hence, DGK-ζ appears to be more important for controlling cellular DAG levels. By contrast, our data suggest that DGK-α plays a modulatory role in shaping the signaling cascade. This functional distinction between the two isoforms is mirrored by differences in their synaptic accumulation patterns. Although initial work in Jurkat cells suggested that DGK-ζ, but not DGK-α, is recruited to

the IS (20), a more recent study in primary T cells has demonstrated that both isoforms do indeed accumulate synaptically (14). We have used TIRF microscopy to extend these observations, and have found that DGK-α localizes preferentially to the periphery of the IS, while DGK-ζ displays a uniform distribution. Together with previous work, our results suggest a model whereby DGK-ζ controls the overall magnitude of DAG signals, while DGK-α controls their subcellular organization. It will be interesting to see if this conceptual distinction is borne out in future studies of isoform specific DGK function in T cells and other cell types.

Although our data indicate that DGK-α controls MTOC polarization by shaping synaptic DAG, we do not exclude a role for DGK-generated PA in this process. Indeed, PA is known to activate PLCγ (30), implying that DGK activity at the IS might actually promote local DAG production. This sort of positive feedback loop could conceivably sharpen the synaptic DAG gradient and enhance the precision of polarization responses. PA can also activate PKCζ (31, 32), an integral component of the PAR (for partitioning defective) polarity complex that includes the adaptor proteins PAR-3 and PAR-6 (33). It was recently shown that PA binds directly to the *drosophila* PAR-3 ortholog Bazooka (34), further suggesting that this complex is regulated directly by PA. Both PAR-3 and PKCζ have been implicated in T cell polarity (35, 36), but precisely how they are coupled to synaptic DAG signaling, if at all, has remained unclear. It is tempting to speculate that PA might function as a molecular link between the two systems.

It initially seemed unlikely that DGK-α could influence MTOC polarization because TCR-induced recruitment of DGK-α to the membrane was thought to require Ca^{2+} signaling (21, 22), and Ca^{2+} is dispensable for polarization responses (4). We have resolved this paradox by demonstrating that PI3K activity drives DGK-α localization to the periphery of the IS. Recently, we showed that PIP_3 is itself enriched in this peripheral domain, where it promotes actin polymerization through the exchange factor Dock2 (26). A direct interaction with this pool of PIP_3 would explain the synaptic accumulation pattern of DGK-α and would be consistent with previous results showing that PIP_3 can stimulate DGK-α activity in vitro (25). It is also possible, however, that PIP_3 controls DGK-α localization via a yet to be defined adaptor complex. Regardless, our results demonstrate that crosstalk between PIP_3 and DAG dependent signaling plays an important role in coordinating cytoskeletal responses downstream of the TCR.

It was somewhat surprising that DGK-$\alpha^{-/-}$ CTLs did not exhibit enhanced cytotoxicity in our hands, despite the fact that their DAG signaling responses were amplified relative to wild type controls. Optimal target cell killing, however, requires not only T cell activation but also proper MTOC reorientation. In the absence of DGK-α, it is likely that the effects of stronger signaling are antagonized by inefficient polarization, yielding little net change in cytotoxicity. This interpretation is consistent with recent data showing that pharmacological inhibition of DGK-α does not enhance CTL functionality unless the protein is overexpressed (37). Our results contrast, however, with a recent report documenting enhanced target cell killing in DGK-$\alpha^{-/-}$ CTLs expressing chimeric antigen receptors (CARs) (15). The experimental system used in this previous study, however, is not strictly comparable to ours. CARs bind their cognate ligands with much higher affinity than TCRs, which presumably

enhances both target cell adhesion and the strength of activating signals. These parameters could certainly influence the relationship between polarity and cytotoxicity. In recent years, the concept of blocking inhibitory regulators like DGK-α in order to augment T cell function during adoptive immunotherapy has received considerable attention (15, 26, 38, 39). It may be useful to keep in mind, however, that suppression of presumed negative regulators in complex signaling networks can have unanticipated results.

The idea that synaptic DAG enrichment requires coordinated production and destruction by PLCγ and DGK-α, respectively, is quite reminiscent of previous work demonstrating that PIP_3 accumulation at the leading edge of migrating cells is maintained by the opposing activities of PI3K and the lipid phosphatase PTEN (40, 41). In both systems, negative regulators act to focus a second-messenger gradient and make it contingent upon continuous activating signals. The polarized signaling that results is highly responsive to minute changes in the orientation and the intensity of receptor stimulation. This conserved strategy is likely to be a common theme in biological systems designed to follow moving targets in complex intercellular environments.

Materials and Methods

Mice

The Institutional Animal Care and Use Committee of Memorial Sloan-Kettering Cancer Center approved the animal protocols used in this study. DGK-$\alpha^{-/-}$ and DGK-$\zeta^{-/-}$5C.C7 TCR-transgenic mice were generated by crossing 5C.C7 TCR-transgenic RAG2$^{-/-}$mice (Taconic) with mice deficient in DGK-α or DGK-ζ, respectively, followed by crossing of the heterozygous progeny. DGK-$\alpha^{-/-}$ OT-1 TCR-transgenic mice were generated by crossing OT-1 TCR-transgenic RAG2$^{-/-}$ mice (Taconic) with DGK-$\alpha^{-/-}$ mice, followed by crossing of the heterozygous progeny.

Cells

$CD4^+$ T cells were isolated from lymph nodes of 5C.C7 TCR-transgenic mice and stimulated with irradiated splenocytes from B10A mice at a ratio 1:5 in the presence of 5 μM MCC. $CD8^+$ T cells were isolated from lymph nodes of OT-1 TCR-transgenic mice and stimulated at a 1:4 ratio with a mixture of irradiated splenocytes from B6 mice pre-incubated with 100 nM OVA. Cells were maintained in RPMI medium containing 10% (vol/vol) FCS, 2 mM L-glutamine, 1 mM sodium pyruvate, nonessential amino acids, 50 U/ml penicillin and 50 μg/ml streptomycin (Invitrogen/Gibco). IL-2 (30 IU/ml) was added 24 h after lymphocyte isolation. $CD8^+$ T cells were split every day and $CD4^+$ T cells were split every two days with complete RPMI containing 30 IU/ml IL-2. CH12 cells and RMA-s cells were cultured in RPMI medium fully supplemented as described above. Phoenix-ECO cells (used for retroviral transduction) were maintained in DMEM supplemented with 10% (vol/vol) FCS, 2 mM L-glutamine, 1 mM sodium pyruvate, nonessential amino acids, 50 U/ml penicillin, and 50 μg/ml streptomycin (Invitrogen/Gibco).

Constructs and retroviral transduction

Full length coding sequences for mouse DGK-α and mouse DGK-ζ isoform 2 were amplified from murine T cell cDNA by PCR and inserted downstream of and in frame with GFP using a TOPO-GFP cloning vector (4). The fusion construct was then transferred into a murine stem cell virus (MSCV) retroviral expression vector. Fragments encoding the ΔEF and ΔEF2C1 constructs were generated by PCR using full length DGK-α cDNA as a template and subcloned into pMSCV as GFP fusions as described above. KD DGK-α, bearing the G432A point mutation, was obtained by two-step PCR mutagenesis as described (42). Centrin-2-RFP, GFP-tubulin and C1θ-GFP constructs have been described (4, 42). Constructs were retrovirally transduced into T cells 72 h or 48 h after initiation of culture for $CD4^+$ T cells or CD8+ T cells, respectively, as previously described (4).

Peptides and proteins

To photocage OVA, a 1-ortho-nitrophenylethyl urethane protecting (NPE) group was installed at the ε-amino position of the p7 Lys. OVA was prepared on resin using standard solid phase peptide synthesis, with Lys 7 incorporated as an ivDde-protected derivative. After chain assembly, the ivDde moiety was selectively removed by hydrazine treatment and the exposed amino group reacted with NPE-N-hydroxysuccinimide ester, prepared as previously described (12). The peptide was cleaved from the resin and globally deprotected using trifluoroacetic acid, and then purified by reversed phase HPLC. H-$2K^b$ heavy chain bearing a C-terminal BirA tags was expressed into inclusion bodies in E. Coli and purified under denaturing conditions. It was then refolded in the presence of excess β2 microglobulin and OVA peptide. After concentration in Millipore ultracentrifugation devices, the samples were biotinylated using the BirA enzyme and further purified by gel filtration chromatography (Superdex 200, GE Pharmacia). The preparation of biotinylated I-E^k-NPE-MCC, I-E^k-MCC, ICAM-1, and B7.1 have been described (12, 43, 44).

ELISA assay

96-well Immuno plates (Nunc) were coated with 10 μg/ml streptavidin in 0.1 M $NaHCO_3$ for 2h, followed by blocking for 2h with 2% (wt/vol) BSA in Hepes-buffered saline (20 mM HEPES, 150mM NaCl). Plates were coated overnight with biotinylated B7.1 (1 μg/ml), ICAM-1 (1 μg/ml) and either I-E^K-MCC (1 μg/ml) or I-E^K-HB (1 μg/ml, nonstimulatory control pMHC). After coating, 1×10^5 5C.C7 T cell blasts were added to the plates. After 16 h at 37 °C, diluted supernatants were added into Immuno plates previously coated with 1 μg/ml anti-mouse IL-2 (clone JES6-1A12, BD Biosciences) antibodies overnight. After 2h incubation of supernatants, plates were washed and incubated an extra 2h with biotinylated anti-mouse IL-2 (clone JES6-5H4, BD Biosciences) antibodies. Plates were then incubated with extra-avidin alkaline phosphatase (dilution 1:1000, Sigma) for 1h and the substrate, pNPP (p-Nitrophenyl Phosphate, Pierce) was added. Plates were read before saturation, a few minutes after addition of the substrate at a wavelength of 405nm.

Biochemical signaling assays

$1–2 \times 10^6$ OT-1 CTLs were preincubated on ice with 5 μg/ml biotinylated anti-CD3 (clone 2C11, eBioscience) and 1 μg/ml biotinylated anti-CD28 (clone 37.51, Biolegend) antibodies.

The antibodies were then crosslinked by addition of 20 μg/ml streptavidin (Peprotech) and incubated at 37ºC. At various time points, 2–4 × 10^5 cells were removed and lysed by incubation in cold lysis buffer (10 mM TrisHCl, 5 mM EDTA, 1 % NP40, 0.5 % sodium deoxycholate, and 0.15 M NaCl, 1 mM sodium fluoride, 0.1 mM orthovanadate, and protease inhibitors). Soluble lysates were analyzed by immunoblot using anti-phospho-Erk1/2 (P-Thr202/Tyr204, clone 20G11, Cell Signaling) and anti-Erk1/2 (clone 137F5, Cell Signaling).

Killing assay

RMA-s target cells were incubated with different concentration of peptides for 45 minutes. Both RMA-s cells and CTLs were washed three times with RPMI supplemented with 1% serum without phenol red. 15,000 RMA-s were incubated with 30,000 T cell blasts per well in 200 μl of medium 1% serum for 5 hours. The release of LDH was measured using the LDH cytotoxicity detection kit (Clontech) according to manufacturer's instructions. All assays were performed in triplicate.

Photoactivation experiments

8 well LabTek chambered coverglass (Nunc) was coated as previously described (12). For 5C.C7 T cells, surfaces were incubated with photocaged I-E^k-NPE-MCC at 0.5 μg/ml, the nonstimulatory pMHC I-E^k-HB at 3 μg/ml, and anti-MHC class I H-$2K^k$ at 0.5 μg/ml (clone 36-7-5, BD Biosciences). For $CD8^+$ T cells, surfaces were coated with 0.1 μg/ml H-$2K^b$-NPE-OVA, 1 μg/ml H-$2D^b$-KAVY, and 1 μg/ml ICAM-1. 2×10^5 T cells were added to each well in imaging medium (RPMI without phenol red medium with 5% FCS and Hepes). In certain experiments, cells were pretreated for 20 min with 0.5 μM wortmannin, 1 μM IC87114, or DMSO (vehicle control) and the drugs were maintained in the medium for the duration of the imaging experiment. 3 s time-lapse series were recorded for 8 min using an inverted fluorescence videomicroscope (Olympus IX-81) equipped with a 150× (NA 1.45) objective lens. Photoactivation was performed using a Mosaic digital diaphragm apparatus (Photonic Instrument) attached to a mercury (HBO) lamp (Olympus). One UV-pulse was performed for 500 ms after 30s of time-lapse recording in order to decage the peptide and deliver the TCR signal. 488 nm or a 564 nm lasers (Melles Griot) were used to image GFP-tagged or RFP-tagged constructs, respectively. MTOC probes (tubulin, centrin) were imaged using epifluorescence illumination, and C1θ using TIRF.

Lipid bilayer experiments

Lipid bilayers were formed in 8-well LabTek chambers as previously described (44). After incubation for 45 min with 20 μg/ml streptavidin, the bilayers were washed and incubated with 1 μg/ml each of biotinylated pMHC (H-$2K^b$-OVA or I-E^k-MCC), ICAM-1, and B7.1 proteins. After bilayer preparation, 2×10^5 T cells transduced with appropriate constructs were added to each well and incubated for 10 min at 37°C prior to fixation for 5 min with 2% paraformaldehyde (PFA). Cells were then permeabilized with 0.5% Triton-X100 for 5 min, blocked with 3% BSA in PBS, and stained for 45 min with Alexa 594 coupled phalloidin (Invitrogen) to visualize F-actin. When necessary, cells were pretreated with 0.5 μM wortmannin or DMSO and drugs were maintained during cell activation. Fixed samples

were imaged on an inverted fluorescence videomicroscope (Olympus IX-81) using 63× (NA 1.45) or 150× (NA 1.45) TIRF objectives.

Conjugate experiments

1×10^5 5C.C7 T cell blasts were mixed with 1×10^5 CH12 target cells, centrifuged at 1500 rpm for 1 min to force conjugate formation, and incubated for 10 min at 37°C. Conjugates were then resuspended in warm PBS, immobilized on polylysine-coated coverslips, and fixed with 2% PFA for 5 min at 37°C. Cells were stained for CD4 using a primary rat anti-mouse CD4 antibody (5 μg/ml, clone GK1.5, eBioscience) and then permeabilized using 0.5% Triton X-100. After blocking with 2% BSA, samples were further stained with polyclonal rabbit anti-mouse pericentrin antibody (5 μg/ml, Abcam), followed by Cy3-labeled donkey anti-rat secondary antibody (1 μg/ml, Jackson Immunoresearch) and FITC-labeled donkey anti-rabbit secondary antibody (1 μg/ml, Jackson Immunoresearch). Fixed samples were imaged using an SP-5 upright confocal microscope (Leica) equipped with a 63× objective.

Image analysis

SlideBook (Intelligent Imaging Innovations, Inc.), ImageJ, and MatLab (MathWorks) software were used for image processing and analysis. MTOC reorientation after photoactivation was quantified by calculating the distance between the center of the irradiated region and the MTOC as a function of time. Polarization histograms were generated using Prism software (GraphPad) by sorting distance measurements from the second half of time-lapse experiments (4–8 min) into 0.2-μm bins (4). Statistical tests of MTOC reorientation data were computed by calculating the mean distance between the MTOC and the irradiated region for each cell during the second half of time-lapse experiments. Conjugate experiments were analyzed by calculating a “polarization index” equal to the distance from the MTOC to the IS divided by the distance from the IS to the distal pole of the T cell. These data were then binned into one of four equally spaced regions starting at the IS and moving towards the distal pole of the T cell (45). To quantify DAG gradient size in lipid bilayer experiments, the fluorescence intensity of C1θ-GFP and F-actin along the line bisecting the IS was computed using ImageJ software. The diameters of the C1θ-GFP and F-actin distributions were determined from this linescan by calculating the distance between the point at which the fluorescence signal reached 50% of its peak intensity above background and the point at which it fell below this 50% threshold. The relative size of the C1θ-GFP gradient relative to the F-actin ring was then expressed as ratio of these diameters. DAG gradient size in photoactivation experiments was determined by calculating the two-dimensional autocorrelation function for each image in the time-lapse (5). Gaussian fitting was then used to determine the characteristic width of the fluorescent signal for each image. Width measurements were normalized to values from the first 10 time points in the experiment (i.e. prior to UV irradiation). Statistical tests of DAG gradient autocorrelation data were computed by calculating the average autocorrelation width for each cell using all time points after UV irradiation. DGK localization in lipid bilayer experiments was analyzed using linescans across the IS. For each linescan, the background-corrected mean fluorescence intensity (MFI) at the edges (positions F1 and F2) of the IS was compared with the background-corrected MFI of three equally spaced central positions (F3,

F4, and F5) as follows: Mean(F3 + F4 + F5)/Mean(F1 + F2). We expect this “clearance ratio” to be ~1 for uniform distributions and <1 for annular patterns.

Statistics

Statistics were calculated using Prism Software. Student’s T-test was used to assess significance in Fig. 5A and 5D. One way ANOVA followed by a Turkey’s multiple comparisons test was used for Fig. 4B, and a Kruskal-Wallis test followed by a Dunn’s Multiple Comparisons test was used for Fig. 6B and Fig. 7B. All other P-values were calculated using the Mann-Whitney test. Data conformity to a Gaussian model was assessed using a D’Agostino & Pearson omnibus normality test.

Supplementary Material

Refer to Web version on PubMed Central for supplementary material.

References

1. Bornens M. The centrosome in cells and organisms. Science. 2012; 335:422. published online EpubJan 27 (335/6067/422 [pii] 10.1126/science.1209037).
2. Huse M, Le Floc’h A, Liu X. From lipid second messengers to molecular motors: microtubule-organizing center reorientation in T cells. Immunol Rev. 2013; 256:95. published online EpubNov (10.1111/imr.12116). [PubMed: 24117815]
3. Spitaler M, Emslie E, Wood CD, Cantrell D. Diacylglycerol and protein kinase D localization during T lymphocyte activation. Immunity. 2006; 24:535. published online EpubMay. [PubMed: 16713972]
4. Quann EJ, Merino E, Furuta T, Huse M. Localized diacylglycerol drives the polarization of the microtubule-organizing center in T cells. Nat Immunol. 2009; 10:627. published online EpubJun. [PubMed: 19430478]
5. Quann EJ, Liu X, Altan-Bonnet G, Huse M. A cascade of protein kinase C isozymes promotes cytoskeletal polarization in T cells. Nat Immunol. 2011; 12:647. published online EpubJul (ni.2033 [pii] 10.1038/ni.2033). [PubMed: 21602810]
6. Krishna S, Zhong XP. Regulation of Lipid Signaling by Diacylglycerol Kinases during T Cell Development and Function. Front Immunol. 2013; 4:178. 10.3389/fimmu.2013.00178). [PubMed: 23847619]
7. Merida I, Avila-Flores A, Merino E. Diacylglycerol kinases: at the hub of cell signalling. The Biochemical journal. 2008; 409:1. published online EpubJan 1. [PubMed: 18062770]
8. Guo R, Wan CK, Carpenter JH, Mousallem T, Boustany RM, Kuan CT, Burks AW, Zhong XP. Synergistic control of T cell development and tumor suppression by diacylglycerol kinase alpha and zeta. Proc Natl Acad Sci U S A. 2008; 105:11909. published online EpubAug 19. [PubMed: 18689679]
9. Olenchock BA, Guo R, Carpenter JH, Jordan M, Topham MK, Koretzky GA, Zhong XP. Disruption of diacylglycerol metabolism impairs the induction of T cell anergy. Nat Immunol. 2006; 7:1174. published online EpubNov (10.1038/ni1400). [PubMed: 17028587]
10. Zhong XP, Guo R, Zhou H, Liu C, Wan CK. Diacylglycerol kinases in immune cell function and self-tolerance. Immunol Rev. 2008; 224:249. published online EpubAug. [PubMed: 18759932]
11. Zhong XP, Hainey EA, Olenchock BA, Jordan MS, Maltzman JS, Nichols KE, Shen H, Koretzky GA. Enhanced T cell responses due to diacylglycerol kinase zeta deficiency. Nat Immunol. 2003; 4:882. published online EpubSep. [PubMed: 12883552]
12. Huse M, Klein LO, Girvin AT, Faraj JM, Li QJ, Kuhns MS, Davis MM. Spatial and temporal dynamics of T cell receptor signaling with a photoactivatable agonist. Immunity. 2007; 27:76. published online EpubJul. [PubMed: 17629516]

13. Dustin ML. Insights into function of the immunological synapse from studies with supported planar bilayers. Curr Top Microbiol Immunol. 2010; 340:1. 10.1007/978-3-642-03858-7_1). [PubMed: 19960306]

14. Joshi RP, Schmidt AM, Das J, Pytel D, Riese MJ, Lester M, Diehl JA, Behrens EM, Kambayashi T, Koretzky GA. The zeta isoform of diacylglycerol kinase plays a predominant role in regulatory T cell development and TCR-mediated ras signaling. Sci Signal. 2013; 6:ra102. 10.1126/scisignal. 2004373). [PubMed: 24280043]

15. Riese MJ, Wang LC, Moon EK, Joshi RP, Ranganathan A, June CH, Koretzky GA, Albelda SM. Enhanced effector responses in activated CD8+ T cells deficient in diacylglycerol kinases. Cancer Res. 2013 published online EpubApr 10 (10.1158/0008-5472.CAN-12-3874).

16. de la Roche M, Ritter AT, Angus KL, Dinsmore C, Earnshaw CH, Reiter JF, Griffiths GM. Hedgehog signaling controls T cell killing at the immunological synapse. Science. 2013; 342:1247. published online EpubDec 6 (10.1126/science.1244689). [PubMed: 24311692]

17. Kupfer A, Dennert G. Reorientation of the microtubule-organizing center and the Golgi apparatus in cloned cytotoxic lymphocytes triggered by binding to lysable target cells. J Immunol. 1984; 133:2762. published online EpubNov. [PubMed: 6384372]

18. Stinchcombe JC, Bossi G, Booth S, Griffiths GM. The immunological synapse of CTL contains a secretory domain and membrane bridges. Immunity. 2001; 15:751. published online EpubNov. [PubMed: 11728337]

19. Tsun A, Qureshi I, Stinchcombe JC, Jenkins MR, de la Roche M, Kleczkowska J, Zamoyska R, Griffiths GM. Centrosome docking at the immunological synapse is controlled by Lck signaling. J Cell Biol. 2011; 192:663. published online EpubFeb 21 (10.1083/jcb.201008140). [PubMed: 21339332]

20. Gharbi SI, Rincon E, Avila-Flores A, Torres-Ayuso P, Almena M, Cobos MA, Albar JP, Merida I. Diacylglycerol kinase zeta controls diacylglycerol metabolism at the immunological synapse. Mol Biol Cell. 2011; 22:4406. published online EpubNov (10.1091/mbc.E11-03-0247). [PubMed: 21937721]

21. Sanjuan MA, Jones DR, Izquierdo M, Merida I. Role of diacylglycerol kinase alpha in the attenuation of receptor signaling. J Cell Biol. 2001; 153:207. published online EpubApr 2. [PubMed: 11285286]

22. Sanjuan MA, Pradet-Balade B, Jones DR, Martinez AC, Stone JC, Garcia-Sanz JA, Merida I. T cell activation in vivo targets diacylglycerol kinase alpha to the membrane: a novel mechanism for Ras attenuation. J Immunol. 2003; 170:2877. published online EpubMar 15. [PubMed: 12626538]

23. Santos T, Carrasco S, Jones DR, Merida I, Eguinoa A. Dynamics of diacylglycerol kinase zeta translocation in living T-cells. Study of the structural domain requirements for translocation and activity. J Biol Chem. 2002; 277:30300. published online EpubAug 16. [PubMed: 12015310]

24. Merino E, Sanjuan MA, Moraga I, Cipres A, Merida I. Role of the diacylglycerol kinase alpha-conserved domains in membrane targeting in intact T cells. J Biol Chem. 2007; 282:35396. published online EpubNov 30. [PubMed: 17911109]

25. Cipres A, Carrasco S, Merino E, Diaz E, Krishna UM, Falck JR, Martinez AC, Merida I. Regulation of diacylglycerol kinase alpha by phosphoinositide 3-kinase lipid products. J Biol Chem. 2003; 278:35629. published online EpubSep 12 (10.1074/jbc.M305635200). [PubMed: 12832407]

26. Le Floc'h A, Tanaka Y, Bantilan NS, Voisinne G, Altan-Bonnet G, Fukui Y, Huse M. Annular PIP3 Accumulation Controls Actin Architecture and Modulates Cytotoxicity at the Immunological Synapse. J. Exp. Med. 2013 in press.

27. Garcon F, Patton DT, Emery JL, Hirsch E, Rottapel R, Sasaki T, Okkenhaug K. CD28 provides T-cell costimulation and enhances PI3K activity at the immune synapse independently of its capacity to interact with the p85/p110 heterodimer. Blood. 2008; 111:1464. published online EpubFeb 1 (blood-2007-08-108050 [pii] 10.1182/blood-2007-08-108050). [PubMed: 18006698]

28. Le Floc'h A, Tanaka Y, Bantilan NS, Voisinne G, Altan-Bonnet G, Fukui Y, Huse M. Annular PIP3 accumulation controls actin architecture and modulates cytotoxicity at the immunological synapse. J Exp Med. 2013; 210:2721. published online EpubNov 18 (10.1084/jem.20131324). [PubMed: 24190432]

29. Zhong XP, Hainey EA, Olenchock BA, Zhao H, Topham MK, Koretzky GA. Regulation of T cell receptor-induced activation of the Ras-ERK pathway by diacylglycerol kinase zeta. J Biol Chem. 2002; 277:31089. published online EpubAug 23. [PubMed: 12070163]
30. Jones GA, Carpenter G. The regulation of phospholipase C-gamma 1 by phosphatidic acid. Assessment of kinetic parameters. J Biol Chem. 1993; 268:20845. published online EpubOct 5. [PubMed: 8407914]
31. Limatola C, Barabino B, Nista A, Santoni A. Interleukin 1-beta-induced protein kinase C-zeta activation is mimicked by exogenous phospholipase D. The Biochemical journal. 1997; 321(Pt 2): 497. published online EpubJan 15. [PubMed: 9020886]
32. Limatola C, Schaap D, Moolenaar WH, van Blitterswijk WJ. Phosphatidic acid activation of protein kinase C-zeta overexpressed in COS cells: comparison with other protein kinase C isotypes and other acidic lipids. The Biochemical journal. 1994; 304(Pt 3):1001. published online EpubDec 15. [PubMed: 7818462]
33. Etienne-Manneville S, Hall A. Cell polarity: Par6 aPKC and cytoskeletal crosstalk. Curr Opin Cell Biol. 2003; 15:67. published online EpubFeb. [PubMed: 12517706]
34. Yu CG, Harris TJ. Interactions between the PDZ domains of Bazooka (Par-3) and phosphatidic acid: in vitro characterization and role in epithelial development. Mol Biol Cell. 2012; 23:3743. published online EpubSep (10.1091/mbc.E12-03-0196). [PubMed: 22833561]
35. Bertrand F, Esquerre M, Petit AE, Rodrigues M, Duchez S, Delon J, Valitutti S. Activation of the ancestral polarity regulator protein kinase C zeta at the immunological synapse drives polarization of Th cell secretory machinery toward APCs. J Immunol. 2010; 185:2887. published online EpubSep 1 (jimmunol.1000739 [pii] 10.4049/jimmunol.1000739). [PubMed: 20679531]
36. Ludford-Menting MJ, Oliaro J, Sacirbegovic F, Cheah ET, Pedersen N, Thomas SJ, Pasam A, Iazzolino R, Dow LE, Waterhouse NJ, Murphy A, Ellis S, Smyth MJ, Kershaw MH, Darcy PK, Humbert PO, Russell SM. A network of PDZ-containing proteins regulates T cell polarity and morphology during migration and immunological synapse formation. Immunity. 2005; 22:737. published online EpubJun. [PubMed: 15963788]
37. Prinz PU, Mendler AN, Masouris I, Durner L, Oberneder R, Noessner E. High DGK-alpha and disabled MAPK pathways cause dysfunction of human tumor-infiltrating CD8+ T cells that is reversible by pharmacologic intervention. J Immunol. 2012; 188:5990. published online EpubJun 15 (10.4049/jimmunol.1103028). [PubMed: 22573804]
38. Loeser S, Loser K, Bijker MS, Rangachari M, van der Burg SH, Wada T, Beissert S, Melief CJ, Penninger JM. Spontaneous tumor rejection by cbl-b-deficient CD8+ T cells. J Exp Med. 2007; 204:879. published online EpubApr 16 (10.1084/jem.20061699). [PubMed: 17403934]
39. Wallner S, Gruber T, Baier G, Wolf D. Releasing the brake: targeting Cbl-b to enhance lymphocyte effector functions. Clinical & developmental immunology. 2012; 2012:692639. 10.1155/2012/692639). [PubMed: 22550535]
40. Devreotes P, Janetopoulos C. Eukaryotic chemotaxis: distinctions between directional sensing and polarization. J Biol Chem. 2003; 278:20445. published online EpubJun 6. [PubMed: 12672811]
41. Merlot S, Firtel RA. Leading the way: Directional sensing through phosphatidylinositol 3-kinase and other signaling pathways. J Cell Sci. 2003; 116:3471. published online EpubSep 1. [PubMed: 12893811]
42. Liu X, Kapoor TM, Chen JK, Huse M. Diacylglycerol promotes centrosome polarization in T cells via reciprocal localization of dynein and myosin II. Proc Natl Acad Sci U S A. 2013; 110:11976. published online EpubJul 16 (10.1073/pnas.1306180110). [PubMed: 23818610]
43. Lillemeier BF, Pfeiffer JR, Surviladze Z, Wilson BS, Davis MM. Plasma membrane-associated proteins are clustered into islands attached to the cytoskeleton. Proc Natl Acad Sci U S A. 2006; 103:18992. published online EpubDec 12. [PubMed: 17146050]
44. Abeyweera TP, Merino E, Huse M. Inhibitory signaling blocks activating receptor clustering and induces cytoskeletal retraction in natural killer cells. J Cell Biol. 2011; 192:675. published online EpubFeb 21 (jcb.201009135 [pii] 10.1083/jcb.201009135). [PubMed: 21339333]
45. Stowers L, Yelon D, Berg LJ, Chant J. Regulation of the polarization of T cells toward antigen-presenting cells by Ras-related GTPase CDC42. Proc Natl Acad Sci U S A. 1995; 92:5027. published online EpubMay 23. [PubMed: 7761442]

46. We thank X. Zhong (Duke University) for mice; the Molecular Cytology Core Facility at MSKCC for confocal microscopy; the Microchemistry Core Facility at MSKCC for peptide synthesis; and R. Joshi (U. Pennsylvania), E. Merino, and members of the Huse and M. O. Li labs for advice. Supported in part by the U. S. National Institutes of Health (R01-AI087644) (M.H.) and the Cancer Research Institute (A. C.)

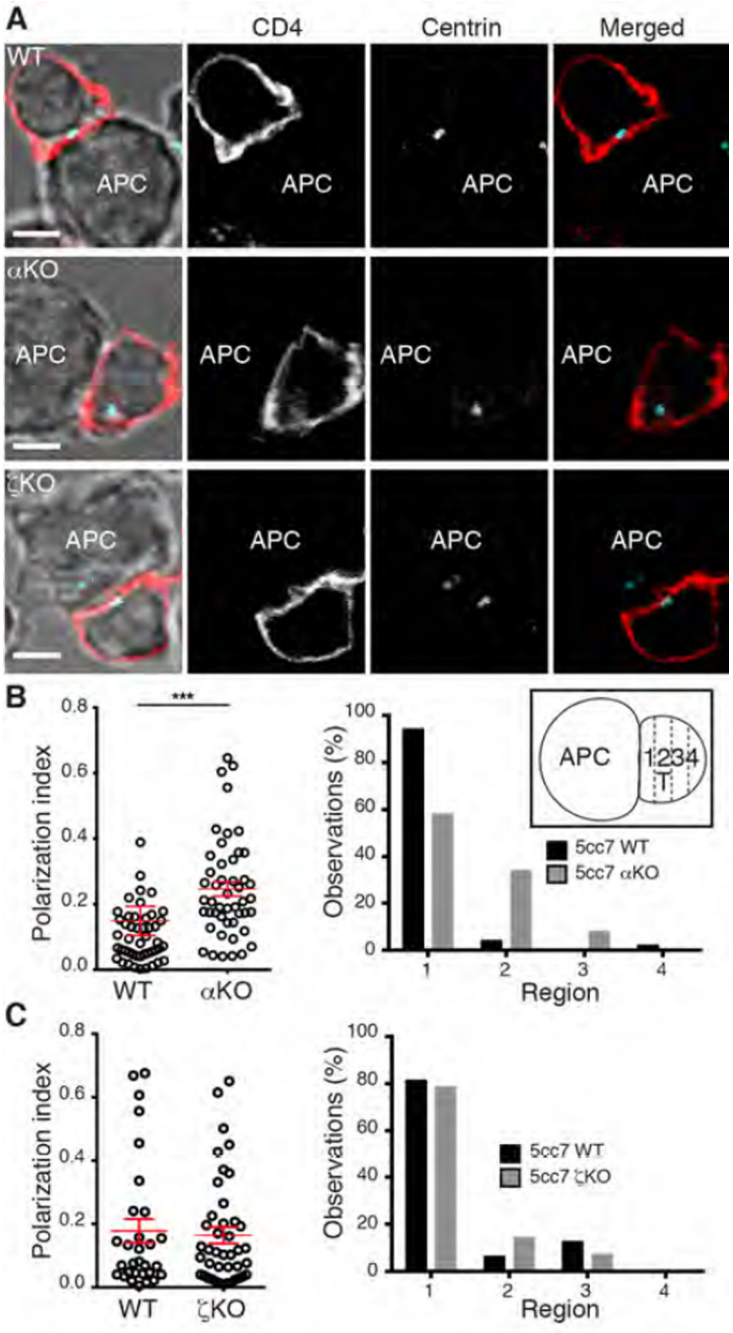

Fig. 1. DGK-α is required for MTOC polarization in T cell-APC conjugates

(A) Wild type (WT) (top), DGK-$\alpha^{-/-}$ (αKO) (middle), or DGK-$\zeta^{-/-}$ (ζKO) (bottom) 5C.C7 T cell blasts were incubated with MCC-loaded CH12 target cells (APC), fixed, and stained with anti-CD4 and anti-pericentrin antibodies. Representative images are shown, with the position of the APC indicated by white text. Scale bars = 10 μm. (B–C) Polarization index (see Materials and Methods) was measured for DGK-$\alpha^{-/-}$ (B, n=48 conjugates) or DGK-$\zeta^{-/-}$ (C, n≥40 conjugates) T cells along with WT controls. In each panel, data are presented in scatter plot format to the left, and in histogram format to the right after binning the data

into four cellular regions proceeding from the IS to the distal pole (represented in the schematic inset in B). Red lines and error bars in scatter plots denote mean and standard error of the mean (s.e.m.), respectively. *** indicates $P < 0.001$. All data are representative of at least two independent experiments.

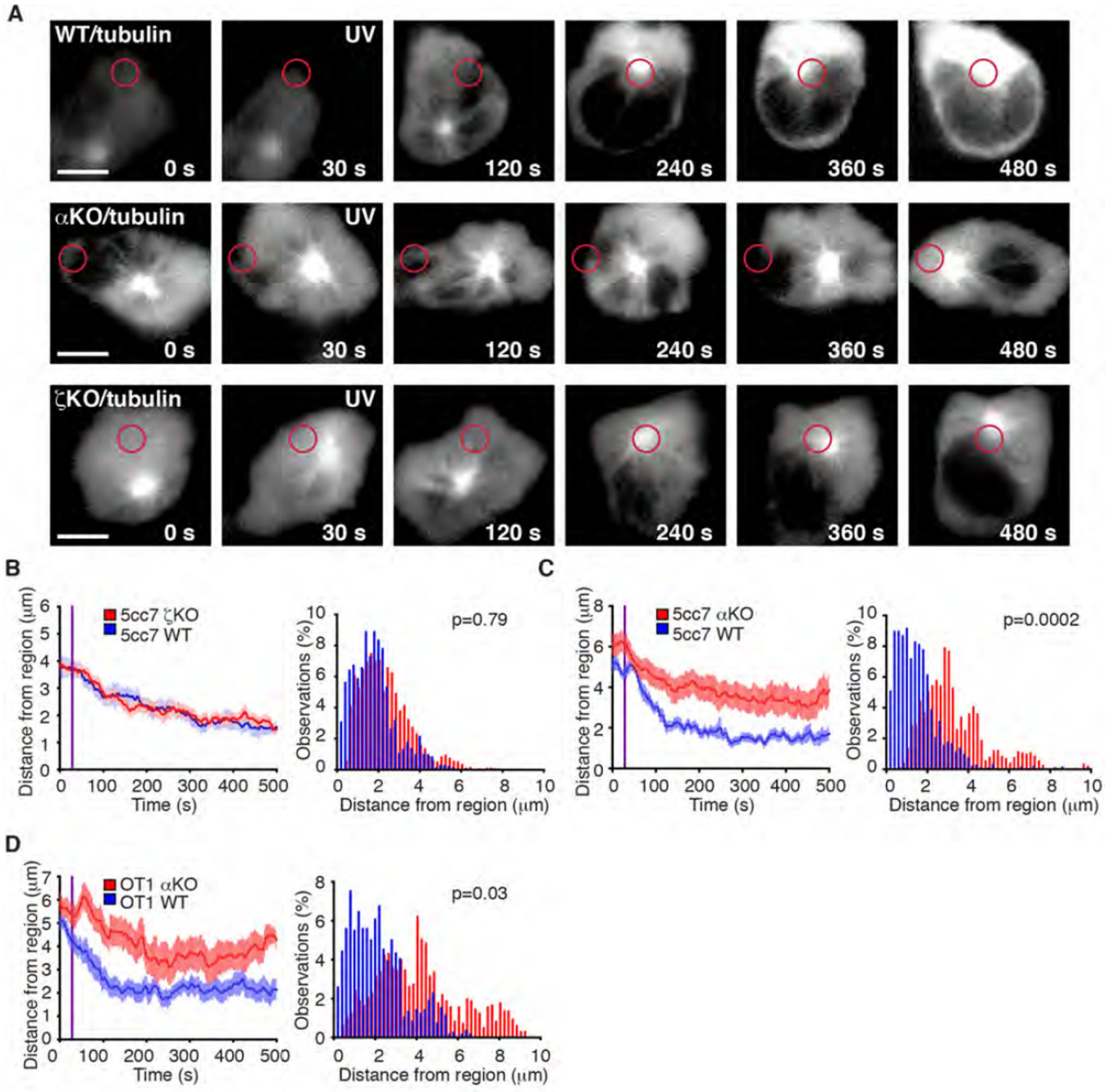

Fig. 2. DGK-α is required for MTOC polarization in TCR photoactivation experiments

(A–C) Wild type (WT), DGK-$\alpha^{-/-}$ (αKO), and DGK-$\zeta^{-/-}$ (ζKO) 5C.C7 T cell blasts expressing GFP-tubulin were imaged and stimulated by localized UV irradiation (red circles) on I-E^k-NPE-MCC coated surfaces. (A) Representative time-lapse montages (WT, top, αKO, middle, ζKO, bottom) are shown, with irradiation time indicated by the appearance of white "UV" text. Scale bars = 10 μm. (B–C) Quantification of MTOC polarization for ζKO (B) and αKO (C) 5C.C7 T cell blasts (n≥16 cells for each condition). Left, average distance between the MTOC and the center of the irradiated region plotted against time, with the purple line indicating UV irradiation. Right, distance measurements

from the second half of all time-lapse experiments (4–8 min) plotted in histogram format. (D) WT or αKO OT-1 CTLs (n=15 cells) were subjected to photoactivation experiments as described in A and the data analyzed as in B and C. Error bars in graphs denote s.e.m. P-values were computed using distance measurements from the second half of each time-lapse. All data are representative of at least four independent experiments.

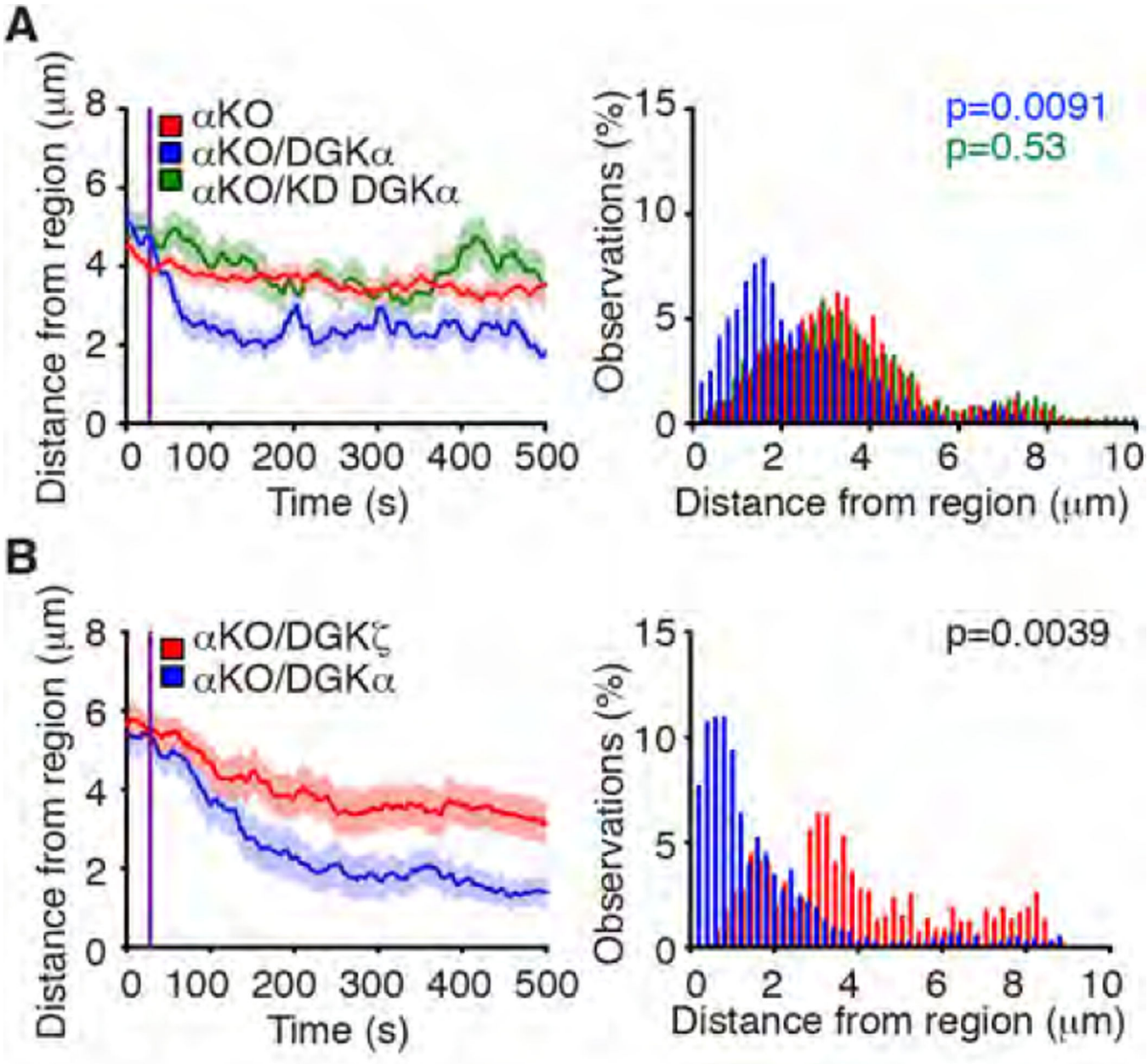

Fig. 3. The DGK-α$^{-/-}$ polarization phenotype is specific

DGK-α$^{-/-}$ (αKO) 5C.C7 T cells expressing GFP-labeled wild type DGK-α (A and B), KD DGK-α (A), or DGK-ζ (B), together with centrin-2-RFP (an MTOC marker) were imaged and stimulated by localized UV irradiation on I-E^{k}-NPE-MCC-coated surfaces. Polarization was analyzed by plotting the distance between the MTOC and the irradiated region as a function of time (left) and by plotting distance measurements from the second half of all time-lapse experiments in histogram format (right). Purple lines indicate UV irradiation, and error bars denote s.e.m. n≥10 cells for each curve. P-values were computed using distance measurements from the second half of each time-lapse. Data are representative of at least two independent experiments.

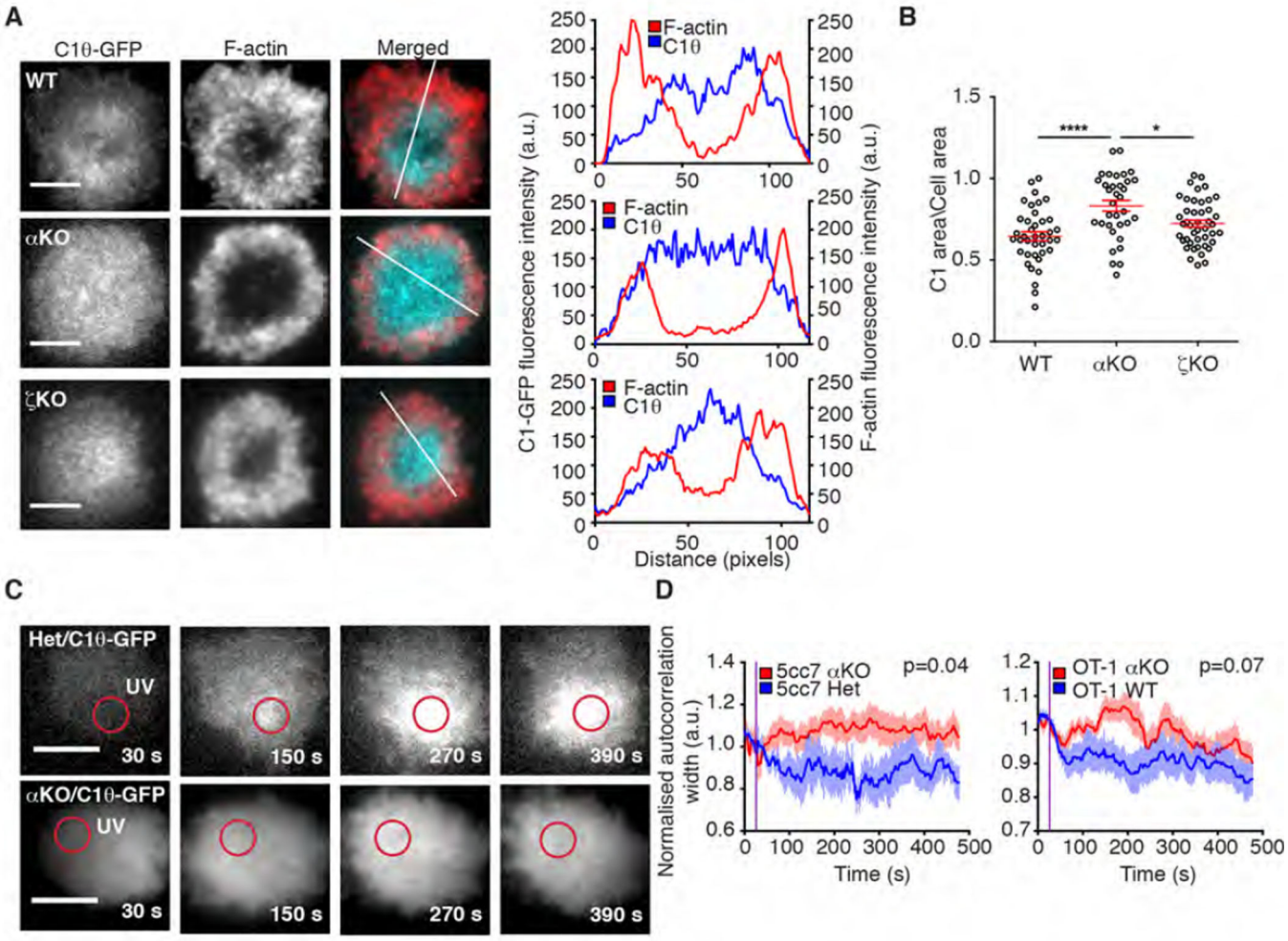

Fig. 4. DGK-α controls the scope of the DAG gradient

(A) Wild type (WT), DGK-$\alpha^{-/-}$(αKO), and DGK-$\zeta^{-/-}$ (ζKO) 5C.C7 T cells were transduced with C1θ-GFP, incubated on lipid bilayers containing ICAM-1, B7.1, and I-E^k-MCC, fixed, and stained for F-actin. Left, representative TIRF images are shown. Right, linescans (derived from the white lines to the left) showing F-actin and C1θ-GFP fluorescence intensity. Scale bars = 10 μm. (B) Quantification of the relative size of DAG accumulation (see Materials and Methods), calculated by normalizing the diameter of the DAG fluorescence signal to the diameter of the F-actin ring (n>30 cells per condition). Red lines and error bars in the scatter plot denote mean and s.e.m., respectively. **** indicates $P < 0.0001$ and * indicates $P < 0.05$. (C) DGK-$\alpha^{+/-}$ (Het) (left) and DGK-$\alpha^{-/-}$ (KO) (right) 5C.C7 T cells expressing C1θ-GFP were imaged and stimulated by localized UV irradiation on I-E^k-NPE-MCC coated surfaces. Representative time-lapse montages are shown, with irradiation time indicated by the appearance of white "UV" text. Scale bars = 10 μm. (D) The average normalized autocorrelation width (see Materials and Methods) of the C1θ-GFP accumulation pattern was plotted against time for both 5C.C7 T cell blasts (left) and OT-1 CTLs (right) (n≥10 cells per curve). Purple lines indicate UV irradiation, and error bars denote s.e.m. P-values in D were computed using averaged autocorrelation measurements

from all time points after UV irradiation. All data are representative of at least two independent experiments.

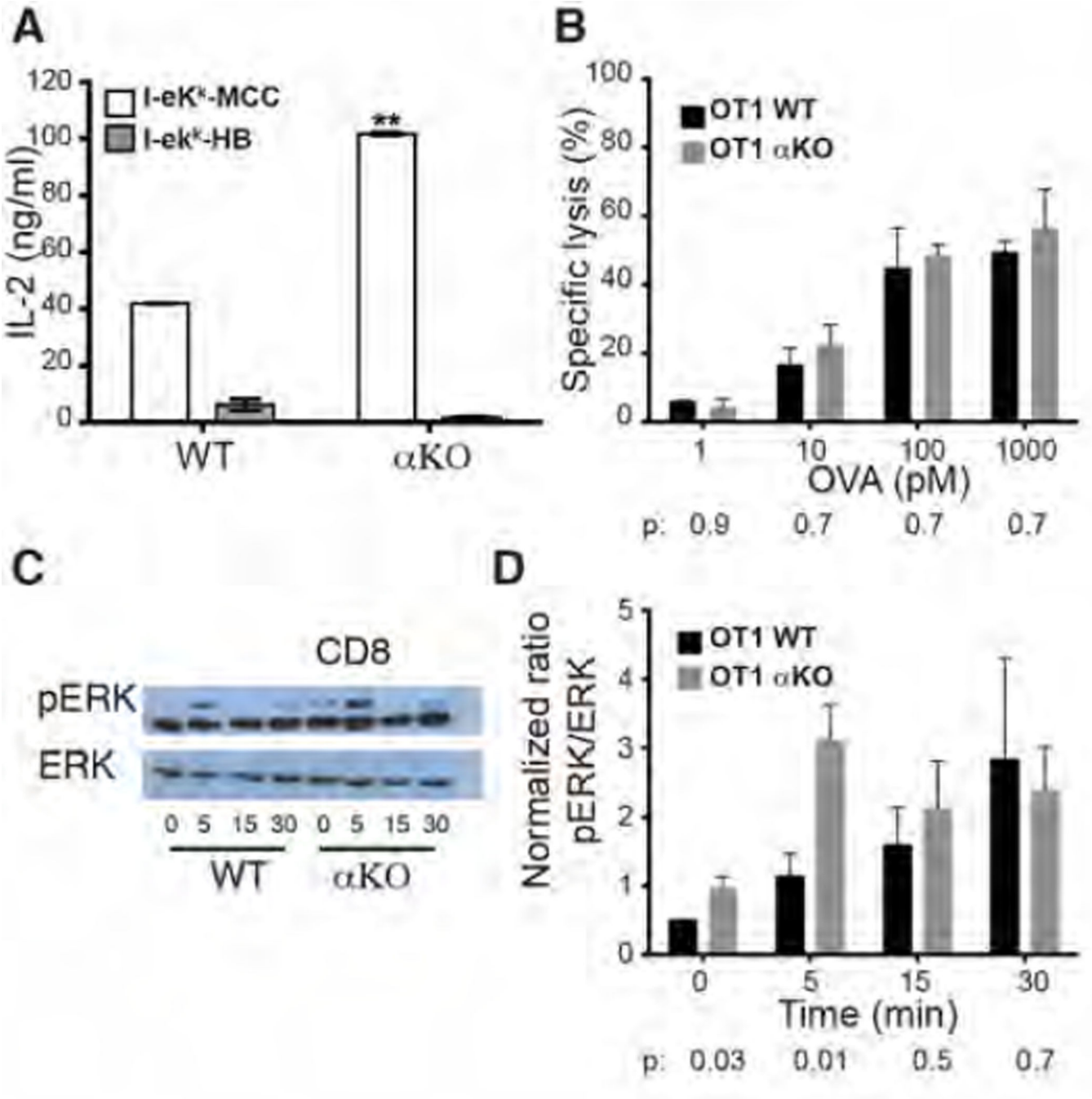

Fig. 5. DGK-α deficiency enhances signaling but not cytotoxicity

(A) WT and αKO T cell blasts were activated on plastic surfaces containing ICAM-1, B7.1, and either stimulatory (MCC) or nonstimulatory (HB) pMHC as indicated. IL-2 secretion was assessed by ELISA. ** indicates $P < 0.01$. (B) WT and αKO OT-1 CTLs were mixed with OVA-loaded RMA-s target cells at an E:T ratio of 2:1. Specific lysis of RMA-s cells is graphed as a function of OVA concentration. Functional assays in A and B were performed in triplicate. Data are representative of at least three independent experiments. (C) DGK-$\alpha^{+/+}$ (WT) and DGK-$\alpha^{-/-}$ (αKO) OT-1 T cell blasts were stimulated by CD3/CD28

crosslinking for the indicated times and pErk1/2 levels assessed by immunoblot. Total Erk was used as a loading control. (D) Quantification of pErk1/2 immunoblot band intensity, using data pooled from three independent experiments. P-values refer to pairwise comparisons between WT and αKO. All error bars denote s.e.m.

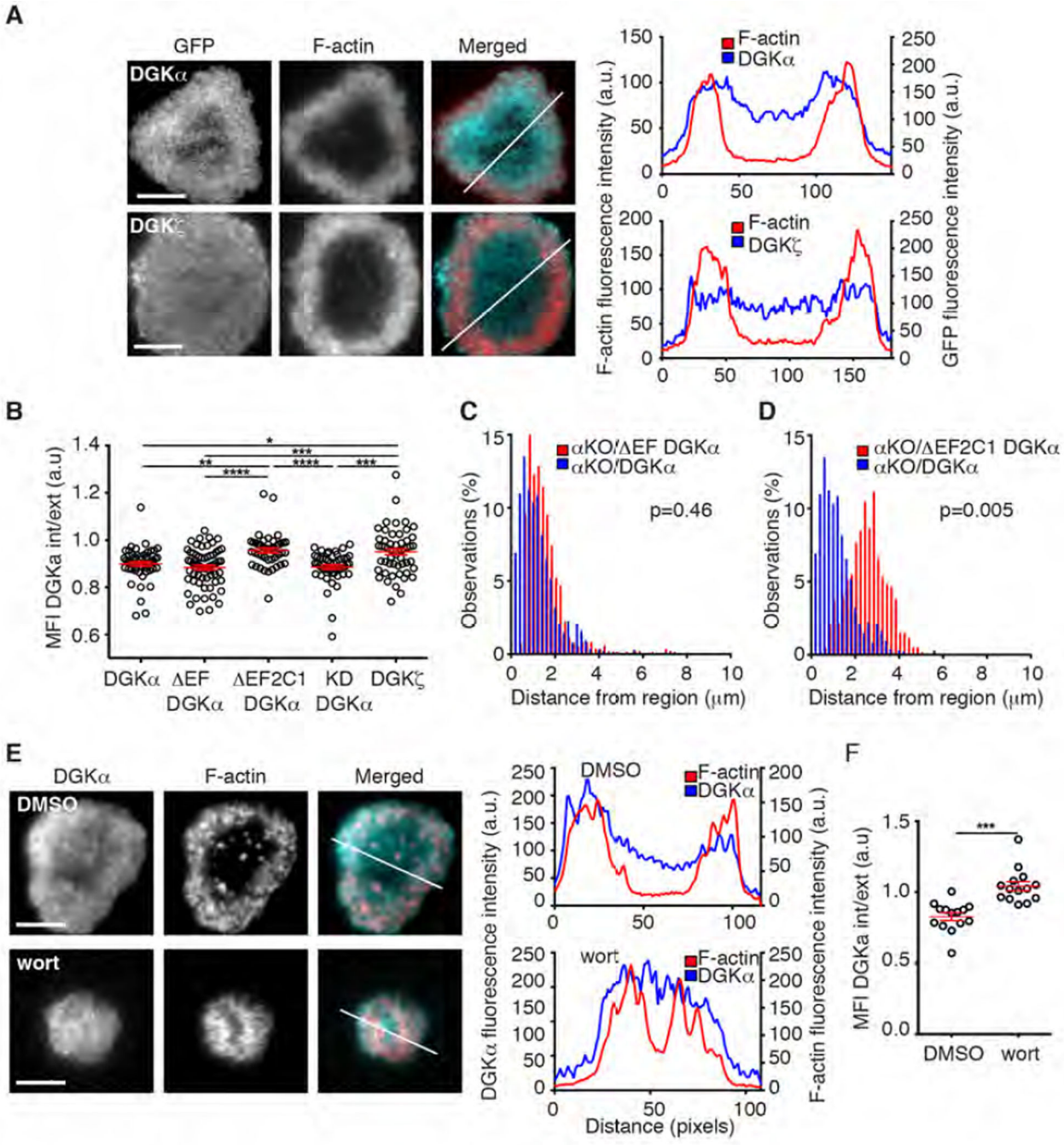

Fig. 6. DGK-α localizes to the periphery of the IS in a PI3K dependent manner

(A) OT-1 CTLs were transduced with GFP-labeled DGK-α or DGK-ζ as indicated, stimulated on bilayers containing H2-K^b-OVA, B7.1, and ICAM-1, fixed, and stained for F-actin. Left, representative TIRF images are shown. Right, linescans (derived from the white lines to the left) showing F-actin and GFP-DGK fluorescence intensity. Scale bars = 10 μm. (B) Quantification of the synaptic localization patterns of the indicated GFP-labeled DGK constructs was performed by comparing the GFP MFI at the center of the IS with the MFI at the periphery (see Materials and Methods) (n≥40 cells per condition). Red lines and error

bars in the scatter plot denote mean and s.e.m., respectively. **** indicates P < 0.0001, ** indicates P < 0.01, and * indicates P < 0.05. (C, D) DGK-α$^{-/-}$ 5C.C7 T cell blasts were transduced with GFP-labeled DGK-α (C, D), ΔEF DGK-α (C), or ΔEF2C1 DGK-α (D) together with centrin-2-RFP. The resulting cells were used in TCR photoactivation experiments to assess MTOC polarization. Results were quantified by plotting distance measurements from the second half of all time-lapse experiments in histogram format (n≥10 cells per condition). P-values were computed using distance measurements from the second half of each time-lapse. (E–F) DGK-α$^{-/-}$ OT-1 CTLs expressing GFP-DGK-α were treated with wortmannin (wort) or DMSO (vehicle control), activated on lipid bilayers containing H-2K^{b}-OVA, ICAM-1, and B7.1, fixed, and stained for F-actin. (E) Left, representative TIRF images are shown. Right, linescans (derived from the white lines to the left) showing F-actin and GFP-DGK-α fluorescence intensity. Scale bars = 10 μm. (F) Synaptic localization of GFP-DGK-α was quantified ratiometrically as in B (n=14 cells per condition). Red lines and error bars in the scatter plot denote mean and s.e.m., respectively. *** indicates P < 0.001. All data are representative of at least three independent experiments.

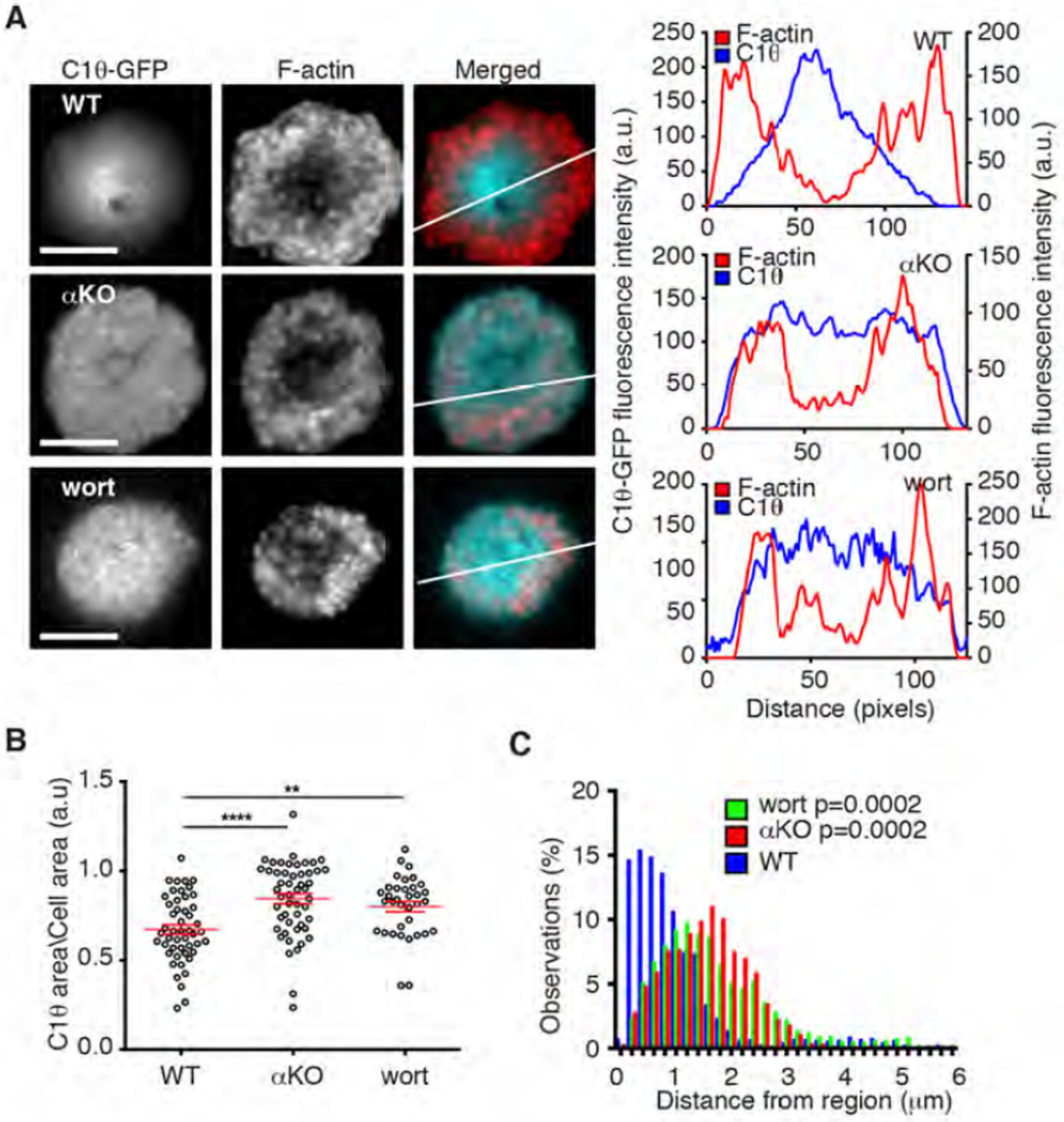

Fig. 7. PI3K activity regulates MTOC polarization and synaptic DAG

(A) Wild type (WT) and DGK-α$^{-/-}$ (αKO) OT-1 CTLs were transduced with C1θ-GFP and incubated on lipid bilayers containing ICAM-1, B7.1 and H-2K^{b}-OVA in the presence or absence of wortmannin (wort) as indicated. Cells were then fixed and stained for F-actin. Left, representative TIRF images are shown. Right, linescans (derived from the white lines to the left) showing F-actin and C1θ-GFP fluorescence intensity. Scale bars = 10 μm. (B) Quantification of the relative size of DAG accumulation, calculated ratiometrically as described in Fig. 4 (n>30 cells per condition). Red lines and error bars in the scatter plot

denote mean and s.e.m., respectively. **** indicates $P < 0.0001$ and ** indicates $P < 0.01$. (C) Wild type (WT) and DGK-$\alpha^{-/-}$ (αKO) OT-1 CTLs were transduced with centrin-2-RFP and subjected to TCR photoactivation experiments in the presence or absence of wortmannin as indicated. Polarization was analyzed by plotting distance measurements from the second half of all time-lapse experiments in histogram format. P-values were computed using distance measurements from the second half of each time-lapse. All data are representative of three independent experiments.